



Paper

Cite this article: Iverson NR, Helanow C, Zoet LK (2020). Debris-bed friction during glacier sliding with ice–bed separation. *Annals of Glaciology* 1–7. <https://doi.org/10.1017/aog.2019.46>

Received: 20 June 2019

Revised: 2 December 2019

Accepted: 3 December 2019

Key words:

Glacier flow; subglacial processes; subglacial sediments

Author for correspondence:

Neal R. Iverson, E-mail: niverson@iastate.edu

Debris-bed friction during glacier sliding with ice–bed separation

Neal R. Iverson¹, Christian Helanow¹ and Lucas K. Zoet²

¹Department of Geological and Atmospheric Sciences, Iowa State University, Ames, IA, USA and ²Department of Geoscience, University of Wisconsin-Madison, Madison, WI, USA

Abstract

Theory and experiments indicate that ice–bed separation during glacier slip over 2-D hard beds causes basal shear stress to reach a maximum at a particular slip velocity and decrease at higher velocities. We use the sliding theory of Lliboutry (1968) to explore how friction between debris particles in sliding ice and a rock bed affects this relationship between shear stress and slip velocity. Particle–bed contact forces and associated debris friction increase with increasing slip velocity, owing to increased rates of ice convergence with up-glacier facing surfaces. However, debris friction on diminished areas of the bed counteracts this effect as cavities grow. Thus, friction from debris alone increases only slightly with slip velocity, and for sediment particles larger than ~60 mm in diameter, debris friction peaks and decreases with increasing slip velocity. The effect on the sliding relationship is to steepen its rising limb and shift its shear stress peak to a slightly higher velocity. These results, which exclude the effect of debris friction on cavity size and debris concentrations above ~15%, indicate that the effect of debris in ice is to increase basal shear stress but not significantly change the form of the sliding relationship.

1. Introduction

The relationship between glacier sliding speed and the shear stress at glacier beds has been a major uncertainty in efforts to model glacier flow for over 60 years (Weertman, 1957). More recently, as interest in ice-sheet response to climate warming has mounted, modeling studies have highlighted the sensitivity of ice loss and sea-level rise projections to the form of the sliding rule (Ritz and others, 2015; Tsai and others, 2015; Brondex and others, 2017; Joughin and others, 2019).

Of many proposed sliding rules, none has greater potential for contributing to fast glacier flow than the one first advocated by Lliboutry (1965, 1968, 1979) in which ice can separate from the lee surfaces of sinusoidal bed undulations. In this case, neglecting regelation, the shear stress increases with steady sliding speed, reaches a maximum, and then decreases over a commonly wide range of sliding speed. This decrease in stress with increasing speed, which we call rate-weakening drag, results from lee side cavities that increase their size with increasing speed; thus, with increasing speed, diminished zones of ice–bed contact on convex bumps are inclined up-glacier at smaller angles, decreasing drag. This model is conceptually in accord with the upper bound on basal shear stress described by Iken (1981) that depends on the maximum adverse slopes of bumps on the bed and effective pressure. Subsequent analyses of sliding with ice–bed separation have been more self-consistent and less heuristic (Fowler, 1986, 1987) and have considered more complicated bed undulations (Schoof, 2005; Gagliardini and others, 2007). These analyses qualitatively affirm the peak in shear stress and rate weakening of Lliboutry's (1968) theory. Moreover, results of laboratory ring-shear experiments with sinusoidal beds demonstrate rate-weakening drag and agree quantitatively with Lliboutry's analysis (Zoet and Iverson, 2015).

However, whether rate-weakening drag associated with cavity growth occurs at glacier beds over length scales large enough to be significant is unknown. Field observations of deglaciated bedrock demonstrate unequivocally that cavities are ubiquitous on hard beds (Walder and Hallet, 1979; Hallet and Anderson, 1980). However, Fowler (1987) and Lliboutry (1987) thought that large bumps on glacier beds not submerged in cavities would prevent rate-weakening drag. Although Schoof (2005) demonstrated that this viewpoint was not necessarily true, he nevertheless advocated a simpler sliding rule in which shear stress, normalized by effective pressure, asymptotically approaches an upper bound without rate weakening.

One motivation for disregarding the rate-weakening drag of sliding theories may come from debris entrained in the basal ice of glaciers. Friction between this debris and the bed contributes to basal shear stress and depends on particle–bed contact forces. In models of debris-bed friction with no ice–bed separation (Hallet, 1981; Shoemaker, 1988), particle–bed contact forces depend on the rate of ice convergence with up-glacier facing (stoss) surfaces during sliding. The resultant component of ice flow toward the bed past particles causes a pressure gradient across them with an associated drag that pushes them against the bed, increasing friction and hence basal shear stress. Ice convergence with surfaces facing up-glacier also occurs when leeward cavities persist at the bed (Iken, 1981). For increasing sliding speeds and cavity sizes, rates of ice convergence and contact forces increase. This increase results from

© The Author(s) 2020. This is an Open Access article, distributed under the terms of the Creative Commons Attribution licence (<http://creativecommons.org/licenses/by/4.0/>), which permits unrestricted re-use, distribution, and reproduction in any medium, provided the original work is properly cited.

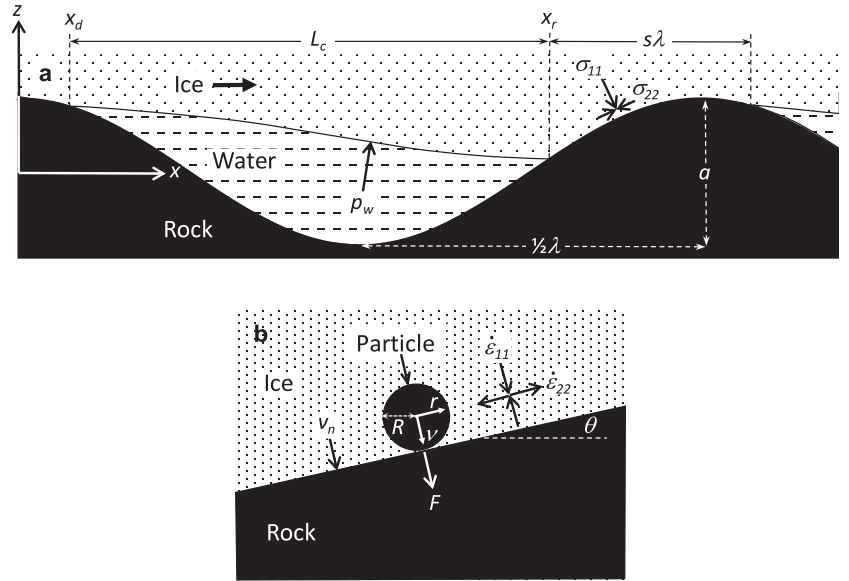


Fig. 1. (a) Model parameters and coordinates for the wavy bed of Lliboutry (1968). (b) Model parameters and coordinates for a particle in frictional contact with the bed over the zone of ice-bed contact, $s\lambda$, in panel (a).

enhanced rates of basal melting and bed-parallel ice extension, caused by increasing normal stresses over diminished zones of ice-bed contact.

This effect motivates the hypothesis we wish to test: that higher particle bed-contact forces at higher slip velocities may lessen or eliminate the rate-weakening drag of sliding models with ice-bed separation (e.g. Lliboutry, 1968; Fowler, 1986). We combine existing theories of clean-ice sliding and of debris-bed friction without ice-bed separation to estimate total basal shear stress as a function of sliding speed. We find that debris-bed friction does not eliminate or significantly reduce rate-weakening drag.

2. Clean ice

In sliding theories, no shear traction acts locally at the bed surface, owing to the water film that divides wet-based glaciers from their beds. Ideally, a local shear traction commensurate with debris-bed friction could be included in such models so that stresses, ice flow and cavity sizes could reflect that friction. Although aspects of this problem have been studied with the finite-element method (Schweizer and Iken, 1992), no analytical model exists that includes local shear tractions and ice-bed separation. Therefore, our tactic is to investigate what insights are possible using existing sliding theory to estimate debris-bed friction, neglecting its feedback on ice flow – a reasonable assumption if shear stress from debris-bed friction is a small fraction of the total basal shear stress.

To analyze sliding with ice-bed separation, we use the theory of Lliboutry (1968) because it enables, in an approximate way, use of a Glen-type, non-linear ice rheology, and because aspects of the theory have been tested experimentally (Zoet and Iverson, 2015). Like most other sliding theories that include ice-bed separation, the theory neglects regelation. This simplification is justifiable because on stoss surfaces where ice is in contact with rock, glacial abrasion generally smooths surfaces (e.g. Hooke, 2005), causing roughness elements as small as the controlling obstacle size (e.g. Weertman, 1957) to be relatively rare. Slip velocity is imposed as an independent variable in the far-field above bumps. No shear traction is allowed locally on the bed surface, owing to the water film, as noted, and the shear traction between water in cavities and cavity roofs is negligibly small. All drag therefore, for the case of clean ice, stems from the distribution of normal stress on the glacier sole exerted by rock in zones of ice-bed contact and by water under pressure in lee side cavities.

Lliboutry (1968) considered a 2-D, rigid bed with a longitudinal profile,

$$z_b = \frac{1}{2} a \cos \frac{2\pi x}{\lambda}, \quad (1)$$

where x is measured parallel to average slope of the bed, a is the bump height from trough to crest, and λ is the wavelength (Fig. 1a). The roughness is $\mathcal{R} = a/\lambda$. Making various approximations, Lliboutry used the bump geometry, slip velocity u , effective pressure, N and the ice flow law parameters to estimate the cavity length, L_c (Fig. 2):

$$L_c = \lambda(1 - s), \quad (2)$$

where s is the fraction of the bed in contact with ice:

$$s = \frac{1}{6\pi\mathcal{R}} \left(\frac{aAN^n}{u} \right)^{1/2}. \quad (3)$$

The flow law of ice is represented by the pre-factor, A , and the creep exponent n (Cuffey and Paterson, 2010, p. 55). Effective pressure $N = \rho g H \cos \alpha - p_w$, where ρ is the ice density, g is the gravitational acceleration, H is the ice thickness, α is the glacier surface slope and p_w is the cavity water pressure. Neglected in deriving Eqn (3) is heat dissipated by water flowing through cavities and resultant melting of cavity roofs; such dissipation is thought to be small in cavities (Walder, 1986). Confidence in this estimate of cavity size comes from Kamb (1987), who considered the same bed geometry and ice rheology and arrived at a similar estimate using a different analysis (Fig. 2).

Also required for estimating basal shear stress is the location, x_d , where the ice detaches from the bed:

$$x_d = \frac{\lambda}{2\pi} \cot^{-1} \left[\frac{2\pi(1-s) + \sin(2\pi s)}{1 - \cos(2\pi s)} \right] \quad (4)$$

(Lliboutry, 1968), where $x_d = 0$ would correspond to ice detachment at the bump crest (Fig. 1a). For increasing sliding speeds, the point of detachment is increasingly close to the bump crest upstream, and the reattachment point, $x_r = x_d + L_c$ (Fig. 1a) approaches the downstream crest (Fig. 3). These results are qualitatively similar to those of Fowler (1986) who considered a linear ice rheology, although in

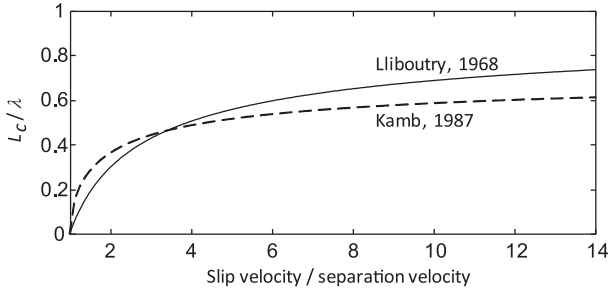


Fig. 2. Cavity length, L_c , scaled by the bed wavelength, λ , as a function of slip velocity scaled by the velocity at which ice separates from lee surfaces, as indicated by the theories of Lliboutry (1968) and Kamb (1987, see his Eqns (8) and (13)).

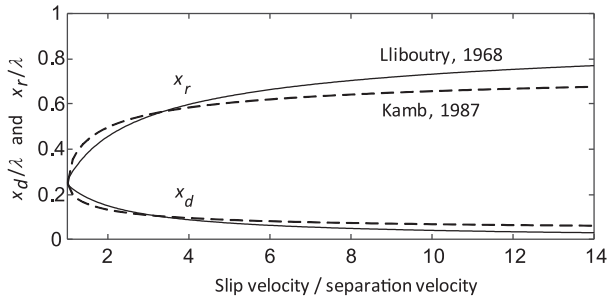


Fig. 3. Points of detachment, x_d , and reattachment, x_r , of ice, as a function of slip velocity scaled by the velocity at which ice separates from lee surfaces, indicated by the theories of Lliboutry (1968) and Kamb (1987). Bump crests are at $x/\lambda = 0$ and $x/\lambda = 1.0$.

his analysis x_d extends slightly up-glacier beyond the bump crest, and the ice reattachment point extends farther down-glacier for a given slip velocity scaled by N and \mathcal{R} .

The basal drag depends on the normal stress, σ_n , that ice exerts on the bed over zones of ice–bed contact. Lliboutry (1968) assumed that this stress varies symmetrically about the centers of such zones where the stress reaches a maximum, to arrive at

$$\sigma_n = p_w - \frac{\pi N}{\sin(\pi s) - \pi s \cos(\pi s)} \left\{ \cos(\pi s) + \cos \left[\frac{2\pi}{\lambda} \left(x - \frac{x_d + x_r}{2} \right) \right] \right\} \quad (5)$$

(see his Eqns (10 and 12)). From this stress distribution, he estimated the basal shear stress, τ , for clean ice:

$$\tau = \frac{1}{2} \pi \mathcal{R} N \left\{ \frac{[\pi s - (1/2) \sin(2\pi s)] \sin(\pi s - (2\pi x_d/\lambda))}{\sin(\pi s) - \pi s \cos(\pi s)} \right\} \quad (6)$$

(Lliboutry, 1968, his Eqns (13 and 14)), where s depends on sliding speed through Eqn (3). The resultant rate-weakening drag (Fig. 4) is qualitatively similar to that determined in subsequent analyses (Fowler, 1986; Schoof, 2005; Gagliardini and others, 2007). A drawback of Lliboutry's model is that he derived separate relationships for sliding velocities below and above the velocity value at which ice–bed separation occurs, resulting in a non-smooth first derivative of the stress relationship at the separation velocity. Thus, Figures 2–4, with sliding velocity scaled by the separation velocity, do not include values <1.0 . This scaling is acceptable because we are concerned with the effect of debris on rate-weakening drag that accompanies cavity growth. The separation velocity can be found from Eqn (3) by setting $s = 1$.

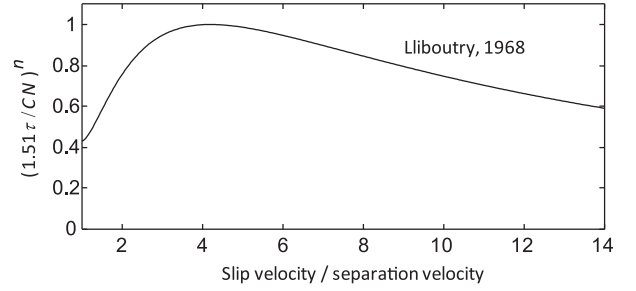


Fig. 4. Sliding rule of Lliboutry (1968) for sliding velocities above those required for ice–bed separation. Shear stress, τ , is scaled following Gagliardini and others (2007) where $C = \pi \mathcal{R}$ is the maximum slope of the bed. The factor, 1.51, adjusts τ to bring it into accord with Iken's (1981) bound. Solving for τ in each of her Eqns (3) and (4) and dividing the results yields this factor; it reflects different assumptions made by Lliboutry (1968) and Iken (1981) regarding the distribution of normal stress on zones of ice–bed contact.

3. Debris-bed friction

Lliboutry's (1968) sliding model allows estimation of rates of ice–bed convergence with stoss surfaces and cavity size as functions of slip velocity. The former controls contact forces between particles and the bed, whereas the latter controls the area of the bed over which debris-bed friction occurs. We wish to explore how the tradeoff between these two variables for different cavity sizes affects the form of the relationship between shear stress and slip velocity.

A major component of ice–bed convergence on stoss surfaces is from extension of ice parallel to the bed as ice flows past bumps (Hallet, 1981). Sliding theory for a sinusoidal bed, in the absence of ice–bed separation and neglecting regelation, yields a component of ice velocity toward the bed everywhere on stoss surfaces at rates that peak at the point midway up stoss surfaces (Nye, 1969, see his Eqn (32) in the limit of zero regelation past bumps). Iken's (1981, her Fig. 6a) numerical calculations of the velocity field in Newtonian ice near a sinusoidal bed for the case of steady cavities similarly demonstrate that a streamline near stoss surfaces converges with the bed and that ice speeds up as it moves down-glacier along zones of ice–bed contact, indicative of bed-parallel extension on stoss surfaces. These facts are also confirmed by recent finite-element simulations of the same process with a Glen-type ice rheology (Helanow and others, 2018). The ubiquity of striations on stoss surfaces (e.g. Hallet, 1979) of large bumps where leeward cavities have been mapped (e.g. Hallet and Anderson, 1980) provides further confirmation that extension of ice parallel to the bed during flow past bumps presses debris particles against stoss surfaces – a process that was first recognized by Gilbert (1906).

This ice extension causes a component of ice velocity toward the bed that is zero at the bed surface but increases away from the bed in the zone of extension. To estimate the bed-normal ice velocity that results from this ice deformation, v_d , we consider the more compressive principal stress, σ_{11} , to be normal to areas of ice–bed contact, following Lliboutry (1968), so $\sigma_{11} = \sigma_n$ (Fig. 1a). A reasonable choice for the less compressive principal stress is $\sigma_{22} = p_w$, the water pressure in cavities, which confines the ice on each side of the zone of ice–bed contact (Fig. 1a). Making these assumptions, defining the mean stress as $p_m = 1/2(\sigma_{11} + \sigma_{22})$, and using Glen's flow law yields the effective strain rate, $\dot{\epsilon}_e$:

$$\dot{\epsilon}_e = A \left\{ \frac{1}{\sqrt{2}} [(\bar{\sigma}_n - p_m)^2 + (p_w - p_m)^2]^{1/2} \right\}^n, \quad (7)$$

where the term in the outermost brackets is the effective shear stress, $(1/2\sigma_{ij}\sigma_{ij})^{1/2}$ (e.g. Hooke, 2005), and $\bar{\sigma}_n$ is the normal stress

(Eqn (5)) averaged over the zone of ice–bed contact. We idealize this strain rate as uniform in the thin zone of ice adjacent to stoss surfaces where debris particles in contact with the bed reside. Noting that $\dot{\epsilon}_e = (1/\sqrt{2})(\dot{\epsilon}_{11}^2 + \dot{\epsilon}_{22}^2)^{1/2}$ and that for the plane strain of this problem, continuity requires $\dot{\epsilon}_{11} = -\dot{\epsilon}_{22}$ (Fig. 1b), then $\dot{\epsilon}_e = \dot{\epsilon}_{11}$. Integrating $\dot{\epsilon}_{11}$ from the bed surface along a coordinate, v , normal to the bed indicates that $v_d = \dot{\epsilon}_{11}v$. The value of v_d that is most relevant to particle–bed contact forces is the velocity at the midpoint of a particle (Hallet, 1981), which corresponds to its radius, R (Fig. 1b). Thus, taking $v = R$, and using Eqn (7) yields the component of ice velocity toward the bed due to the bed-parallel extension of ice:

$$v_d = \frac{AR}{2^{n/2}} [(\bar{\sigma}_n - p_m)^2 + (p_w - p_m)^2]^{n/2}. \quad (8)$$

The other component of bed-normal ice velocity results from basal melting. The heat flux dissipated by sliding ice is $q_s = \tau u$. We assume that all of this heat flux and the geothermal heat flux, q_G , melt ice only along the ice–bed contacts where ice is coldest, so the rate of basal melting, v_m , depends on cavity size through s :

$$v_m = \frac{1}{s\rho L}(q_G + \tau u). \quad (9)$$

As in the derivation of Eqn (3), heat dissipated by water flowing through cavities is neglected. Equations (8) and (9) provide the total bed-normal ice velocity, v_n (Fig. 1b) in zones of ice–bed contact: $v_n = v_d + v_m$.

Contact force, F , exerted normal to the bed by particles in zones of ice–bed contact, depends on v_n because as ice moves toward the bed it exerts a bed-normal drag on particles (Fig. 1b). Watts (1974) determined the drag on an isolated sphere exerted by temperate ice moving by regelation and enhanced creep. Hallet (1979, 1981) adapted this result and added to it the sphere’s buoyant weight in ice to obtain

$$F = \frac{f4\pi\eta_e R^3}{R_*^2 + R^2} v_n + \frac{4}{3}\pi R^3 g(\rho_r - \rho) \cos \theta, \quad (10)$$

where η_e is the effective viscosity of ice, R_* is the controlling particle size, f is an empirical factor >1.0 that accounts for the accentuating effect of the bed proximity on drag, ρ_r is the particle density and θ is the angle between the local bed slope and horizontal (Fig. 1b). Particle buoyant weight, as indicated by the right-hand term, is a significant fraction of F only for $R > 0.1$ m (Hallet, 1979). Experiments with inclusions in ice in which v_n has been measured indicate that drag indeed depends on v_n (Iverson, 1990; Byers and others, 2012), with $f \approx 2.0$ (Byers and others, 2012). Cavities that form in these spaces between particles and the bed led Boulton (1974) to suggest that the difference between the ice pressure and water pressure in these cavities controlled contact forces. However, water pressure in cavities of steady size beneath isolated particles on the bed must be at least slightly higher than the mean ice pressure to enable drainage from cavities through the water film along the bed surface to ‘connected’ parts of the subglacial hydraulic system. We thus use Eqn (10) to estimate contact forces but acknowledge that it is contingent on the assumption that water produced by melting along particle surfaces drains through the water film at the ice–rock interface. Equally important is that Eqn (10) applies only to debris particles that are sufficiently isolated from each other that their flow fields do not interact.

Owing to the power-law rheology of ice, η_e and R_* in Eqn (10) depend on v_n . The effective viscosity depends on the flow-law parameters:

$$\eta_e = \frac{\dot{\epsilon}_{rv}^{(1/n-1)}}{2A^{1/n}}, \quad (11)$$

where r is the distance from particle centers parallel to the local bed slope and remembering that v is the coordinate perpendicular to the local bed slope (Fig. 1b). Approximating η_e therefore requires choosing a reference value of the shear strain rate, $\dot{\epsilon}_{rv}$. Neglecting bed-normal gradients in velocity parallel to the local bed slope, $\dot{\epsilon}_{rv} = (1/2)(\delta v_n/\delta r)$. The radial variation in bed-normal velocity, δv_n , is at most v_n . Taking $\delta v_n = v_n$, and choosing δr as the particle diameter, $2R$, then yields

$$\dot{\epsilon}_{rv} = \frac{v_n}{4R}. \quad (12)$$

The resultant value of effective viscosity from Eqn (11) determines in Eqn (10) the value of R_* :

$$R_* = \left(\frac{3\eta_e C_m K}{\rho L} \right)^{1/2}, \quad (13)$$

where C_m is the melting point depression with pressure, and K is a bulk thermal conductivity of particles and ice (Watts, 1974).

From the contact force, F , and fractional area of ice–bed contact, s , the component of bed shear stress due to debris-bed friction, τ_d , is

$$\tau_d = sC\mu F \cos \theta, \quad (14)$$

where C is the concentration of particles in contact with the bed (particle number per unit area), μ is the coefficient friction between rock particles and the bed and $\cos \theta$ isolates the component of stress parallel to the average bed slope, assumed to be zero. Eqn (14) may overestimate τ_d because particles may rotate in ice under a torque smaller than the torque, μFR , caused by full mobilization of clast-bed friction. We neglect this complication to maximize the possible effect of debris-bed friction on the sliding rule. For the same reason we consider only maximum values of C , limited by the requirement that debris particles be widely enough spaced so that flow fields around them do not interact. Velocity distributions in ice during its power-law flow past an isolated sphere (Llibouty and Ritz, 1978) indicate that particles separated by at least ~ 1.5 particle diameters satisfy this criterion. This spacing of particles at the bed surface implies that the number of particles per unit area of the bed is

$$C = \frac{1}{6.25\pi R^2}. \quad (15)$$

If the same particle spacing applies normal to the bed, then the associated concentration of debris in ice by mass is $\sim 15\%$.

Equations (3–5) and (8–13) allow estimation of contact forces and areas of ice–bed contact as a function of sliding speed, and Eqn (14) provides the resulting estimate of debris-bed friction, maximized for each particle size through Eqn (15). Table 1 shows relevant parameter values.

4. Results

The bed-normal component of ice velocity, v_n , in zones of ice–bed contact – the driver for particle–bed contact forces – increases with increasing velocity and cavity size but at a decreasing rate

Table 1. Parameter values

Symbol	Parameter	Value ^a
A	Pre-factor of ice flow law	$2.41 \times 10^{-24} \text{ Pa}^{-3} \text{ s}^{-1}$
C_m	Melting point depression with pressure	$7.4 \times 10^{-8} \text{ K Pa}^{-1}$
f	Drag enhancement factor for particles on bed	2.0
K	Bulk thermal conductivity of particles and ice	$5.6 \text{ W m}^{-1} \text{ K}^{-1}$ ^b
L	Latent heat of fusion of ice	$3.34 \times 10^5 \text{ J kg}^{-1}$
μ	Particle-bed coefficient of friction	0.6^c
n	Creep exponent of ice flow law	3.0
q_G	Geothermal heat flux	0.065 W m^{-2} ^d
ρ	Density of ice	900 kg m^{-3}
ρ_r	Density of rock	2700 kg m^{-3} ^c

^aValues from Cuffey and Paterson (2010) unless noted otherwise here or in the text.

^bWatts (1974).

^cJaeger and Cook (1979).

^dPollack and others (1993).

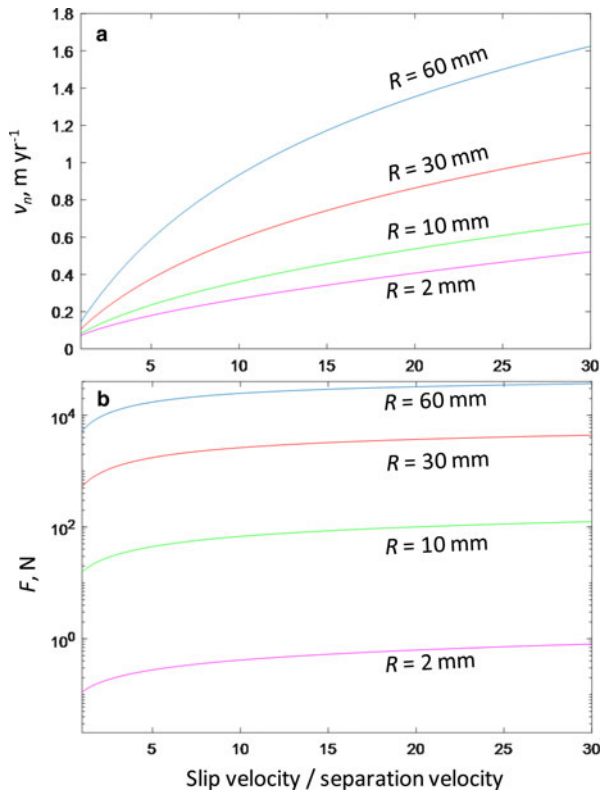


Fig. 5. (a) Convergence velocity, v_n , and (b) contact force, F , for different particle radii, R . Bed roughness, $\mathcal{R} = 0.1$ and effective pressure, $N = 500 \text{ kPa}$. This value of N , for the case of basal water pressure at 80% of the ice overburden pressure, corresponds to a glacier $\sim 280 \text{ m}$ thick.

for various particle sizes (Fig. 5a). The normal stress on the bed (Eqn (5)) and the associated rate of ice extension on stoss surfaces are largely responsible for this variation, which reflects cavity growth rate decreasing with increasing slip velocity (Fig. 2). Large particles extend higher in the ice and thus are subjected to larger values of ice-bed convergence from ice extension than smaller particles (Fig. 5a). Contact forces (Eqn (10)) increase similarly with slip velocity (Fig. 5b), but contact forces vary orders-of-magnitude more with particle size than do bed-normal ice velocities. This large variation reflects little drag on small particles due to the efficiency of regelation and much larger drags on larger particles closer to the controlling particle size ($R_* = 0.03\text{--}0.15 \text{ m}$, depending on v_n and R , Eqns (11–13)). The effect of a given particle size on debris-bed friction also depends, however, on the particle concentration in ice, which is larger for smaller particles (Eqn (15)). Considering the product, CF , of the particle concentration and contact force indicates that larger particles,

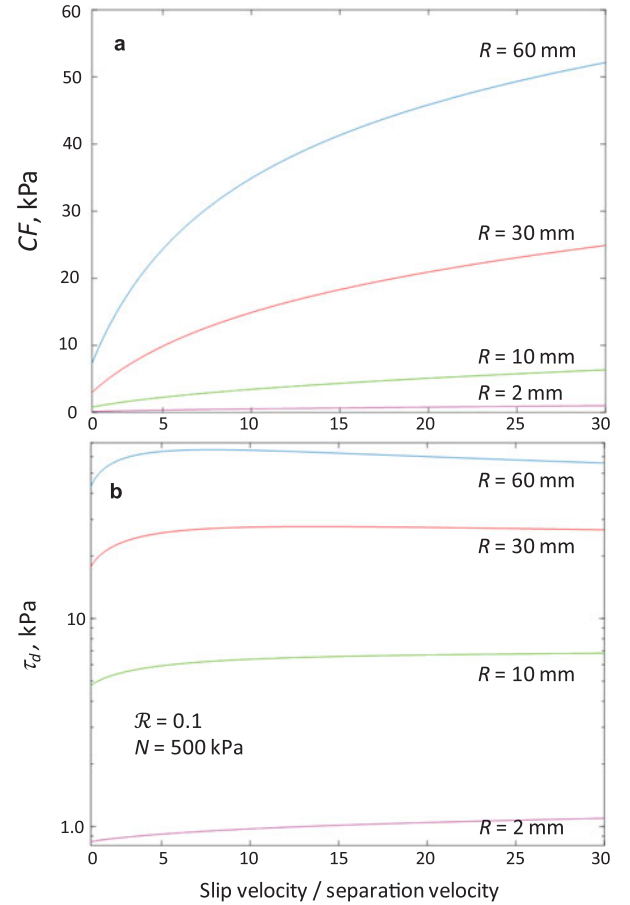


Fig. 6. (a) The product of contact force, F , and debris concentration, C (in particles per m^2), and (b) the shear stress caused by debris-bed friction, for different particle radii, R . Bed roughness, $\mathcal{R} = 0.1$, and effective pressure, $N = 500 \text{ kPa}$.

nevertheless, have a significantly larger effect on total contact forces than smaller particles (Fig. 6a).

Debris-bed friction, therefore, increases with increasing particle size (Fig. 6b). Regardless of particle size, the sensitivity of debris-bed friction to slip velocity is small, owing to growth of cavities with increasing slip velocity, as factored into Eqn (14) through the fractional area of ice-bed contact, s . Interestingly, debris-bed friction does not monotonically increase with slip velocity for all particle sizes. For the two largest particle sizes considered, at a sufficiently high slip velocity debris-bed friction reaches a maximum and declines at still higher slip velocities. This behavior reflects the rapid decrease in the rate at which CF increases with slip velocity for larger particles (Fig. 6a), causing high sensitivity of debris-bed friction to changing cavity size that reverses the slope of the relationship for larger particles.

However, apart from increasing the magnitude of the basal shear stress, the overall effect of debris-bed friction on the form of the sliding rule is small (Fig. 7). Debris-bed friction steepens the ascending limb of the sliding rule and slightly increases the threshold slip velocity at which the peak shear stress occurs, thus reducing the propensity for rate-weakening drag. These effects are minor, however, because decreases in ice-bed contact area with cavity growth mute or reverse the effect of increases in debris-bed friction from increased contact forces. Note that in Figure 7 drag depends on chosen values of bed roughness (0.1) and effective pressure (500 kPa). Although the shear stress scaling for clean ice is independent of these variables (Fig. 4), in Figure 7 we do not use this scaling because it is inappropriate when shear stress depends, in part, on debris friction.

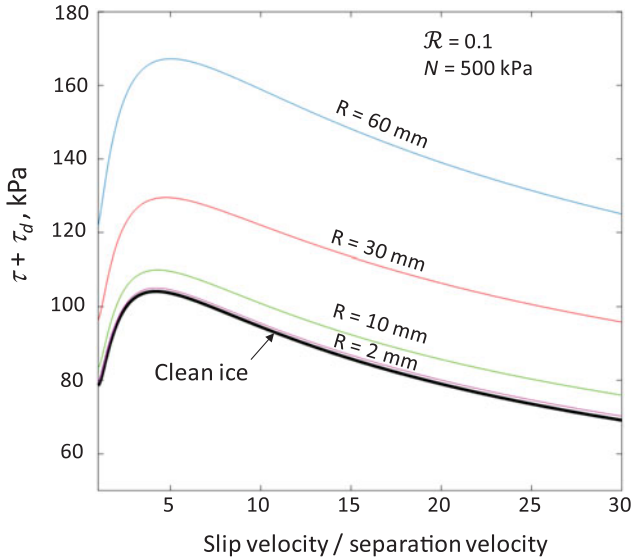


Fig. 7. Sum of shear stress with clean ice, τ , and with debris-bed friction, τ_d , for different particle radii, R . Bed roughness, $\mathcal{R} = 0.1$ and effective pressure, $N = 500$ kPa.

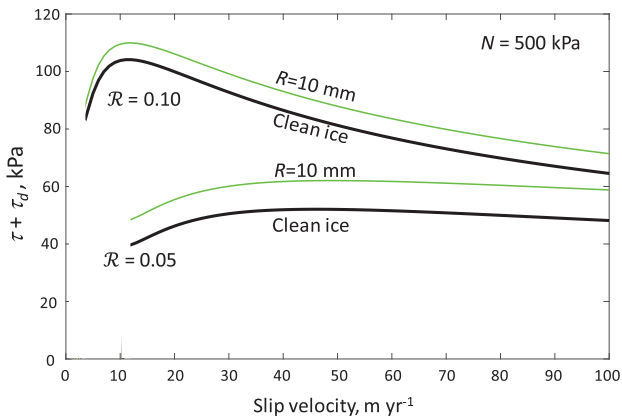


Fig. 8. Sum of shear stress with clean ice, τ , and shear stress from debris-bed friction, τ_d , for two values of bed roughness, \mathcal{R} . Particle radius, $R = 10$ mm, and effective pressure $N = 500$ kPa.

Dependencies of the friction-influenced sliding rule on bed roughness and effective pressure, shown in plots in which both shear stress and slip velocity are unscaled (Figs 8 and 9), further illustrate the importance of cavity size. Smaller bed roughness (Fig. 8), in addition to decreasing the peak stress and the magnitude and velocity range of rate-weakening drag, increases the component of stress due to debris-bed friction. This reflects smaller cavities and larger areas of the bed over which debris-bed friction acts if roughness is low. For the same reason, debris-bed friction increases with increasing effective pressure (Fig. 9), which reduces cavity size. For small but reasonable values of effective pressure (e.g. 300 kPa), threshold slip velocities for ice–bed separation can be extremely low, and rate-weakening drag can occur over nearly the full range of possible slip velocity. Debris-bed friction does little to alter this effect (Fig. 9).

5. Discussion and conclusions

Increasing cavity size with increasing slip velocity has two opposing effects on debris-bed friction. Larger cavities increase normal stresses on zones of ice–bed contact, with associated higher rates of ice-convergence and contact forces. Larger cavities also,

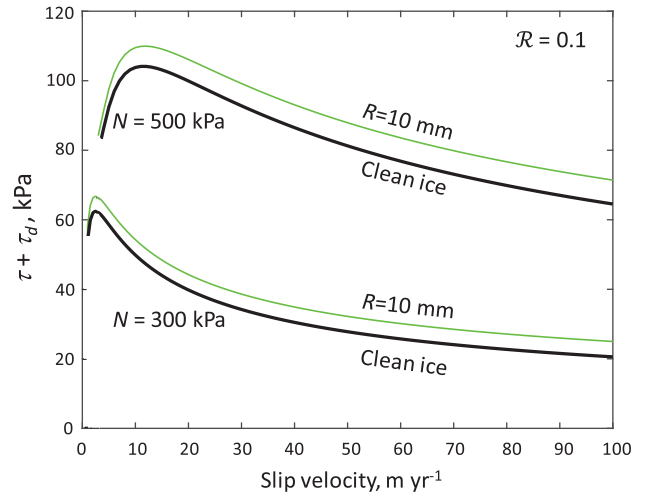


Fig. 9. Sum of shear stress with clean ice, τ , and shear stress from debris-bed friction, τ_d , for two values of effective pressure, N . Particle radius, $R = 10$ mm, and bed roughness, $\mathcal{R} = 0.1$.

however, reduce the area over which debris-bed friction acts. For all particle sizes, the combination of these effects at low slip velocities causes debris-bed friction to increase with increasing velocity. For sufficiently large particles, debris-bed friction peaks, with rate-weakening friction at higher velocities (Fig. 6). The effect of debris-bed friction on basal shear stress is to steepen the rising limb of the sliding rule and shift the peak in drag to a slightly larger slip velocity (Fig. 7). However, the overall sensitivity of debris-bed friction to sliding speed is sufficiently small that these effects on the form of the sliding rule are minor.

In principle, debris can substantially increase the peak stress (Fig. 7), but accurately estimating this stress has not been our goal. We have maximized debris concentrations without specifying reasonable ranges of particle size. For example, a collection of grapefruit-sized clasts ($R = 60$ mm, Figs 5–7) with $3R$ spacing (Eqn (15)) at the bed is unlike any grain-size distribution observed in the basal ice of a glacier. Rather, our goal has been to ask, with debris-bed friction maximized, whether it can have a significant effect on the form of the sliding rule. The answer, within the limitations of the analysis, is no, and that answer should also apply to realistic grain-size distributions in which large particles are few relative to small particles.

Limitations of the analysis include neglecting the effect of debris friction on sliding speed and cavity size and neglecting debris concentrations in ice sufficiently large so that ice flow fields around particles interact. The former is neglected because no analytical model of sliding with ice–bed separation exists for the case of a non-zero shear traction applied at the bed surface, although Morland (1976) considered this problem. Including this effect might influence the tradeoff between contact forces and cavity size with sliding speed. Dense concentrations of debris particles in ice are not common but sometimes observed. A speculation, based on one set of laboratory experiments with dense debris in temperate ice (Iverson, 1993), is that micro-cavities beneath adjacent particles merge so that an irregular water layer, much thicker than the normal water film, exists at the bed surface. If this layer were hydraulically transmissive enough for water pressure within it to be controlled by the pressure in the subglacial hydraulic system, effective pressure could become the dominant control variable for contact forces. In this case, particle–bed contact forces could be much higher than for the case of sparse debris.

These results indicate that debris-bed friction does not eliminate or significantly lessen rate-weakening drag indicated by

idealized theories and experiments, leaving open the major question of how actual hard beds may suppress rate weakening. One possibility is that some bumps on glacier beds may be both large enough to remain unsubmerged in cavities and have stoss faces that are steeper than those already submerged (Schoof, 2005). Alternatively, on actual glacier beds bump crests may align too poorly along a flowline for cavities to submerge stoss surfaces sufficiently under the operative range of sliding speed (Zoet and Iverson, 2016). Also, the degree of convexity of stoss surfaces in contact with ice could be important. Development of sliding theory for realistic, 3-D bedrock surfaces, therefore, might allow the physics of hard-bedded sliding to be reconciled with large-scale glacier flow models that neglect rate-weakening drag.

Alternatively, such theory might show that rate-weakening drag on actual hard beds is not suppressed and so point to a major inadequacy in how the basal boundary condition in glacier flow models is handled. As discussed previously (Lliboutry, 1968; Fowler, 1987; Schoof, 2005), a glacier with a bed that effectively becomes slipperier with increasing slip velocity would be inherently prone to fast flow and associated mass losses.

Acknowledgements. This work was supported by a grant to NRI and LKZ from the US National Science Foundation (EAR-1660972). We thank reviewers, J.S. Walder and T. Creyts, and scientific editor, M. Truffer, for helpful comments.

References

- Boulton GS** (1974) Processes and pattern of glacial erosion. In Coates DR (ed.), *Glacial Geomorphology*. Binghamton, NY: State University of New York, pp. 41–87.
- Brondeix J, Gagliardini O, Gillet-Chaulet F and Durand G** (2017) Sensitivity of grounding line dynamics to the choice of the friction law. *Journal of Glaciology* **63**(241), 854–866. doi.org/10.1017/jog.2017.51
- Byers J, Cohen D and Iverson NR** (2012) Subglacial clast/bed contact forces. *Journal of Glaciology* **58**(207), 89–98. doi.org/10.3189/2012JoG11J126
- Cuffey KM and Paterson WSB** (2010) *The Physics of Glaciers*, 4th Edn, Oxford: Butterworth-Heinemann.
- Fowler AC** (1986) A sliding law for glaciers of constant viscosity in the presence of subglacial cavitation. *Proceedings of the Royal Society of London A* **407**, 147–170.
- Fowler AC** (1987) Sliding with cavity formation. *Journal of Glaciology* **33**(115), 255–267.
- Gagliardini O, Cohen D, Råback P and Zwinger T** (2007) Finite-element modeling of subglacial cavities and related friction law. *Journal of Geophysical Research*, **112**, 1–11. doi.org/10.1029/2006JF000576
- Gilbert GK** (1906) Crescentic gouges on glaciated surfaces. *Bulletin of the Geological Society of America* **17**(9), 303–316.
- Hallet B** (1979) A theoretical model of glacial abrasion. *Journal of Glaciology* **23**(89), 39–50.
- Hallet B** (1981) Glacial abrasion and sliding: their dependence on the debris concentration in basal ice. *Annals of Glaciology* **2**, 23–28.
- Hallet B and Anderson RS** (1980) Detailed glacial geomorphology of a proglacial bedrock area at Castleguard Glacier, Alberta, Canada. *Zeitschrift fuer Gletscherkunde und Glazialgeologie* **16**(2), 171–184.
- Helanow C, Iverson NR and Zoet LK** (2018) Sliding rule for glacier slip with cavities over a 3D bed. *American Geophysical Union Fall Meeting (C44A-04)*.
- Hooke RLB** (2005) *Principles of Glacier Mechanics*, 2nd Edn, Cambridge: Cambridge University Press.
- Iken A** (1981) The effect of subglacial water pressure on the sliding velocity of a glacier in an idealized numerical model. *Journal of Glaciology* **27**(97), 407–421.
- Iverson NR** (1990) Laboratory simulations of glacial abrasion: comparison with theory. *Journal of Glaciology* **36**(124), 304–314.
- Iverson NR** (1993) Regelation of ice through debris at glacier beds: implications for sediment transport. *Geology* **21**, 559–562.
- Jaeger JC and Cook NGW** (1979) *Fundamentals of Rock Mechanics*, 3rd Edn, New York: Chapman and Hall.
- Joughin I, Smith BE and Schoof CG** (2019) Regularized Coulomb friction laws for ice sheet sliding: application to Pine Island Glacier, Antarctica. *Geophysical Research Letters* **46**(9), 4764–4771. doi.org/10.1029/2019GL082526
- Kamb B** (1987) Glacier surge mechanism based on linked cavity configuration of the basal water conduit system. *Journal of Geophysical Research* **92**, 9083–9100.
- Lliboutry L** (1965) *Traité de Glaciologie, Tom. 2*. Paris: Masson et Cie.
- Lliboutry L** (1968) General theory of subglacial cavitation and sliding of temperate glaciers. *Journal of Glaciology* **7**(49), 21–58.
- Lliboutry L** (1979) Local friction laws for glaciers: a critical review and new openings. *Journal of Glaciology* **23**(89), 67–95.
- Lliboutry L** (1987) Realistic, yet simple bottom boundary conditions for glaciers and ice sheets. *Journal of Geophysical Research* **B92**(9), 9101–9110.
- Lliboutry L and Ritz C** (1978) Ecoulement permanent d'un fluide visqueux non linéaire (corps de Glen) autour d'une sphère parfaitement lisse. *Annales Geophysicae* **34**(2), 133–146.
- Morland LW** (1976) Glacier sliding down an inclined wavy bed with friction. *Journal of Glaciology* **17**(77), 463–477.
- Nye JF** (1969) A calculation on the sliding of ice over a wavy surface using a Newtonian viscous approximation. *Proceedings of the Royal Society of London* **311**(1506), 445–467.
- Pollack HN, Hurter SJ and Johnson JR** (1993) Heat flow from the Earth's interior: analysis of the global data set. *Reviews of Geophysics* **31**(3), 267–280.
- Ritz C and 5 others** (2015) Potential sea-level rise from Antarctic ice-sheet instability constrained by observations. *Nature* **528**, 115–118. doi.org/10.1038/nature16147
- Schoof C** (2005) The effect of cavitation on glacier sliding. *Proceedings of the Royal Society of London* **461**, 609–627. doi.org/10.1098/rspa.2004.1350
- Schweizer J and Iken A** (1992) The role of bed separation and friction in sliding over a deformable bed. *Journal of Glaciology* **38**(128), 77–92.
- Shoemaker EM** (1988) On the formulation of basal debris drag for the case of sparse debris. *Journal of Glaciology* **34**(118), 259–264.
- Tsai VC, Stewart AL and Thompson AF** (2015) Marine ice-sheet profiles and stability under Coulomb basal conditions. *Journal of Glaciology* **61**(226), 205–215. doi.org/10.3189/2015JoG14J221
- Walder JS** (1986) Hydraulics of subglacial cavities. *Journal of Glaciology* **32** (112), 439–445.
- Walder JS and Hallet B** (1979) Geometry of former subglacial water channels and cavities. *Journal of Glaciology* **23**(89), 335–346.
- Watts PA** (1974) *Inclusions in Ice* (PhD thesis). University of Bristol.
- Weertman J** (1957) On the sliding of glaciers. *Journal of Glaciology* **3**(21), 33–38.
- Zoet LK and Iverson NR** (2015) Experimental determination of a double-valued drag relationship for glacier sliding. *Journal of Glaciology* **61**(225), 1–7. doi.org/10.3189/2015JoG14J174
- Zoet LK and Iverson NR** (2016) Rate-weakening drag during glacier sliding. *Journal of Geophysical Research: Earth Surface* **121**, 1206–1217. doi.org/10.1002/2016JF003909.